

# Quasiparticle self-consistent $GW$ study of $\text{LaNiO}_3$ and $\text{LaNiO}_3/\text{LaAlO}_3$ superlattice

Myung Joon Han\*

*Department of Physics and KAIST Institute for the NanoCentury,  
Korea Advanced Institute of Science and Technology, Daejeon 305-701, Korea*

Hiori Kino

*National Institute for Materials Science, Sengen 1-2-1, Tsukuba, Ibaraki 305-0047, Japan.*

Takao Kotani

*Department of Applied Mathematics and Physics, Tottori University, Tottori 680-8552, Japan  
(Dated: February 21, 2014)*

Using quasiparticle self-consistent  $GW$  calculations we examined the electronic structure of  $\text{LaNiO}_3$  and the  $\text{LaNiO}_3/\text{LaAlO}_3$  superlattice. The effects of electron correlation in Ni- $d$  bands were reasonably well described without any *ad hoc* parameter and without the ambiguity related to the double-counting and downfolding issues. The effective mass is about 30% enhanced compared to the GGA result. One band feature, which is believed to be essential for the cuprate-like superconductivity, is not realized and the central Fermi surface pocket does not disappear. Our result is consistent with a recent dynamical mean field calculation based on the  $d$ - $p$  model and in contrast to the result from a  $d$ -band only model.

PACS numbers: 75.70.Cn, 73.20.-r, 75.47.Lx, 71.15.Mb

## I. INTRODUCTION

Recently nickelate superlattices have attracted considerable attention, especially due to the reported possibility of high-temperature superconductivity. A recent dynamical mean field theory (DMFT) calculation reported that the band structure of  $\text{LaNiO}_3/\text{LaAlO}_3$  (LNO/LAO)-type heterostructure can be cuprate-like [1] while another DMFT calculation based on a Hubbard Hamiltonian explicitly containing oxygen  $p$  bands made a different prediction [2]. Also, an intriguing metal-insulator transition (MIT) accompanied by magnetic transition was observed [3].

From the theoretical point of view, it is a great challenge to describe the correct ground state of LNO as well as a LNO/LAO superlattice based on the first-principles method. Conventional LDA or GGA overestimates the bandwidth and underestimates the effective mass while the correct paramagnetic (PM) ground state is reproduced for LNO [4]. This limitation is clearly manifested when it is applied to LNO/LAO. While LNO/LAO becomes magnetic and insulating in the thin LNO limit [3, 5–7], LDA/GGA still gives a PM and metallic ground state [8]. Since the LDA+ $U$  type of approach strongly prefers the magnetic ground state, it yields a local moment at the Ni site in the LNO/LAO, consistent with experiments in the thin LNO limit [3], but the problem is that LDA+ $U$  cannot describe the correlated PM phase. As a result, for the thick LNO limit of the superlattice and for bulk LNO, LDA+ $U$  predicts a ferro- (or antiferro-) magnetic ground state, which is in sharp contrast with

the reality [9]. Although DMFT is one of the ways to go beyond LDA+ $U$  especially for the correlated PM phase, there is a discrepancy between two DMFT results for the Fermi surface topology of the LNO/LAO superlattice as mentioned above [1, 2]. This demonstrates the limitation of the current DMFT scheme as an ideal first-principles electronic structure calculation method. The ambiguities inevitably arise from the downfolding, projection,  $U$  and  $J$  parameters, and double-counting terms. From this perspective, the nickelate superlattice is an archetypal example that challenges the predictive power of current first-principles methods to simulate correlated electron systems.

Here we take an alternative approach, namely, the quasiparticle self-consistent  $GW$  (QSGW) method. Without any *ad hoc* parameter, QSGW gives a reasonable band structure in terms of the bandwidth and the effective mass both for LNO and the superlattice. Importantly, our calculation shows that the band structure of LNO/LAO does not become cuprate-like, which supports the conclusion of the DMFT result based on the  $d$ - $p$  model.

## II. COMPUTATION METHOD

### A. Quasiparticle self-consistent $GW$ method

The QSGW was originally introduced by Faleev, van Schilfhaarde and Kotani [10], and has now become a widely used standard method with which one can calculate  $H_0$  (non-interacting Hamiltonian describing quasiparticles (QPs) or band structures) and  $W$  (dynamically-screened Coulomb interactions between the QPs within the random phase approximation (RPA)) in a self-

---

\*Electronic address: mj.han@kaist.ac.kr

consistent manner. Note that QSGW fully takes into account the non-locality of the one-particle potential. This feature is distinctive from DMFT, in which the non-locality connecting different atomic sites is often missing, whereas dynamical effects can be incorporated with the one-particle potential.

While the one-shot  $GW$  is a perturbative calculation starting from a given  $H_0$  (usually from the  $H_0$  of Kohn-Sham Hamiltonian in GGA/LDA), QSGW is a self-consistent perturbation method that can determine the one-body Hamiltonian within itself. To be clearer, let us recall that the  $GW$  approximation gives the one-particle effective Hamiltonian whose energy dependence comes from the self-energy term  $\Sigma(\omega)$  (here we omit index of space and spin for simplicity). In QSGW, the static one-particle potential  $V^{\text{xc}}$  is generated from  $\Sigma(\omega)$  as

$$V^{\text{xc}} = \frac{1}{2} \sum_{ij} |\psi_i\rangle \{ \text{Re}[\Sigma(\varepsilon_i)]_{ij} + \text{Re}[\Sigma(\varepsilon_j)]_{ij} \} \langle \psi_j|, \quad (1)$$

where  $\varepsilon_i$  and  $|\psi_i\rangle$  refer to the eigenvalues and eigenfunctions of  $H_0$ , respectively, and  $\text{Re}[\Sigma(\varepsilon)]$  is the Hermitian part of the self-energy [10–12]. With this  $V^{\text{xc}}$ , one can define a new static one-body Hamiltonian  $H_0$ , and continue to apply  $GW$  approximation until converged. In principle, the final result of QSGW does not depend on the initial conditions. Previous QSGW studies, ranging from semiconductors [11, 12] to the various 3d transition metal oxides [11–13] and 4f-electron systems [14], have demonstrated its capability in the description of weakly and strongly correlated electron materials.

## B. Computation details

We used our new implementation of QSGW [15] by adopting the ‘augmented plane wave (APW) + muffin-tin orbital (MTO)’, designated by ‘PMT’ [16, 17], for the one-body solver. The accuracy of this full potential PMT method is proven to be satisfactory in the supercell calculations of homo-nuclear dimers from  $\text{H}_2$  through  $\text{Kr}_2$  with the significantly low APW energy cutoff of  $\sim 4$  Ry by including localized MTOs [17]. A key feature of this scheme for QSGW is that the expansion of  $V^{\text{xc}}$  can be made with MTOs, not APWs, which enables us to make the real space representation of  $V^{\text{xc}}$  at any  $\mathbf{k}$  point. It can therefore be similar to another implementation of QSGW based on the maximally localized Wannier functions [18]. Also, in contrast to a previous approach based on FP-LMTO (full potential linearized muffin-tin orbital) [12], our scheme is free from the fine tunings of MTO parameters. The basis set for the eigenfunctions can be enlarged systematically with the APW cutoff and no empty sphere is required.

The lattice constant used for LNO (cubic perovskite) is 3.86 Å. For  $(\text{LNO})_1/(\text{LAO})_1$ , the in-plane lattice is set to be 3.905 Å (SrTiO<sub>3</sub> value as the substrate) while the  $c$

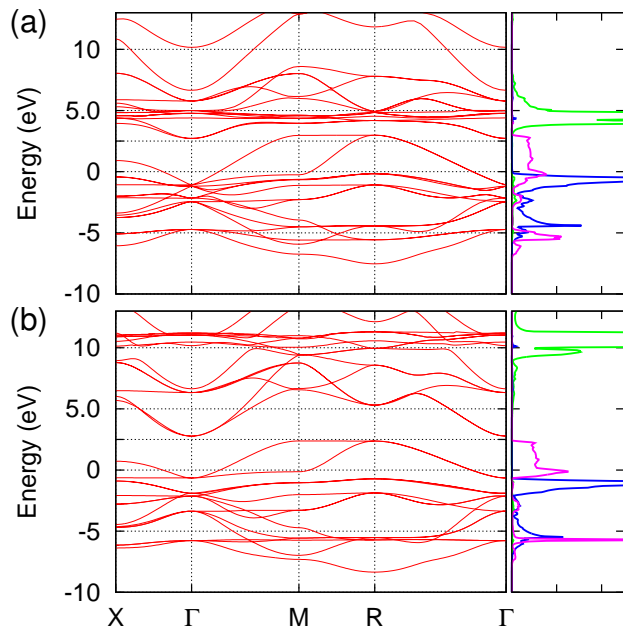


FIG. 1: The calculated band dispersion of bulk LNO by (a) GGA and (b) QSGW. The Fermi level is set to be 0. The PDOS is also presented in the right panel in which the blue, magenta, and green lines refer to the Ni- $t_{2g}$ , Ni- $e_g$ , and La-4f states, respectively. The radii of the MT spheres are 1.02 and 1.59 Å for Ni and La, respectively.

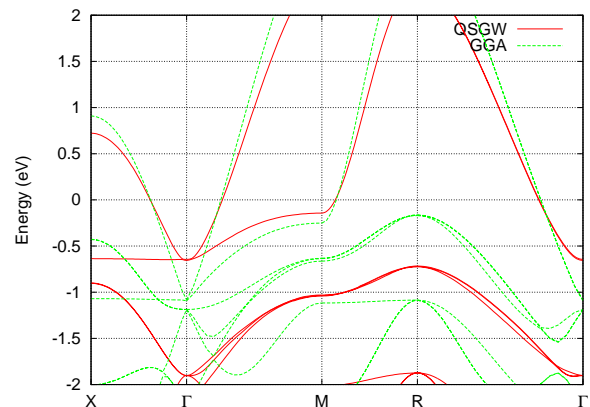


FIG. 2: The band dispersion of LNO near the Fermi level calculated by GGA (dashed green) and QSGW (solid red). The Fermi level is set to be 0.

lattice parameter and the internal atomic positions were optimized with GGA. We assumed that the tetragonal symmetry is preserved and that rotational or breathing-type distortion does not occur because enlarging the unit-cell requires too much computation cost for our QSGW calculation. Since such distortions can be realized and the oxygen cage rotations generally reduce hopping, the correlation effect in our calculation might be underestimated as discussed further below. We used  $8 \times 8 \times 4 = 256$

System	$m_{\text{QSGW}}/m_{\text{GGA}}$		$N_{e_g}$	
	Electron	Hole	GGA	QSGW
LNO	1.36	1.43	2.16	2.04
LNO/LAO	1.39	1.29	2.15	2.04

TABLE I: The calculated electron/hole mass ( $m_{\text{QSGW}}/m_{\text{GGA}}$ ) and the number of  $e_g$  electrons ( $N_{e_g}$ ) for LNO and LNO/LAO. For the effective mass of LNO, the  $\Gamma$  to (R, M, X) and R to ( $\Gamma$ , M, X) lines are taken for the electron and hole mass, respectively, and the average values are presented. For LNO/LAO,  $\Gamma(\text{M})$  to (X(X), M( $\Gamma$ )) and Z(A) to (A(R), R(Z)) lines are taken for electron (hole).

and  $8 \times 8 \times 8 = 512$   $\mathbf{k}$  points for the self-energy calculation in the first Brillouin zone of  $(\text{LNO})_1/(\text{LAO})_1$  and LAO, respectively. The convergency of the present results is robust against the change of the number of  $\mathbf{k}$  points and the other cutoff parameters.

### III. RESULT AND DISCUSSION

#### A. Electronic structure of $\text{LaNiO}_3$

As a prototype example that shows the limitation of the conventional first-principle methodologies, bulk LNO has been examined by several advanced methods. For example, Deng *et al.* [19] applied their LDA+DMFT to bulk cubic LNO. Gou *et al.* performed a comparative study using LDA, GGA, LDA+ $U$  and hybrid functional [20].

Our result is presented in Fig. 1. The band structure obtained by QSGW is markedly different from GGA. First of all, the Ni- $e_g$  bandwidth is notably reduced. The antibonding part of the Ni- $e_g$  dispersion reaches up to 3.0 eV in GGA result (Fig. 1(a)) while it is 2.4 in QSGW (Fig. 1(b)). The bandwidth reduction is about  $\sim 1.2$  eV. This result clearly shows that the QSGW captures the correlation effect which is poorly described by the conventional LDA/GGA type of approach. Another notable difference is that two  $e_g$  bands across the Fermi level are completely decoupled from the other bands in QSGW, which is not the case in GGA. The bonding part is also affected. In GGA, the bonding combination of Ni- $e_g$  is located in between  $-4.8$  and  $-7.5$  eV (Fig. 1(a)) whereas, in QSGW, it is in between  $-5.8$  and  $-8.3$  eV (Fig. 1(b)). For the bonding part, the bandwidth change is not significant while the location is pushed down [21]. The  $t_{2g}$  complex is also slightly changed by QSGW.

The bandwidth reduction and the electronic correlation captured by QSGW are important for determining material properties since the effective mass is enhanced accordingly. It is found that the effective electron and hole mass calculated by QSGW are about 40 % larger than GGA values (Table I).

Notable changes are also found in the higher energy regions. The La-4*f* bands located at  $\sim 5$  eV in GGA are pushed away by QSGW. Since the unphysical energy position of La-4*f* significantly affects material properties (*e.g.*, bond length and binding energy), this fea-

ture should be corrected in the LDA+ $U$  or +DMFT approach. It causes another ambiguity in determining the additional parameters for La-*f* orbitals (or other rare-earth elements) besides the transition metal *d*. In this regard, therefore, QSGW has a clear advantage with no adjustable parameter [22]. Relatively deep core level bands (at around  $-15$  eV or below; not shown) are found to be pushed down by a few electron volts in QSGW results which can be important for interpreting, for example, the X-ray spectroscopic data related to such a level position.

It is instructive to compare our QSGW result with the previous DMFT by Deng *et al.* [19]. For this purpose, we present the enlarged band dispersion around the Fermi level in Fig. 2. The downshift of  $t_{2g}$  bands (just below the anti-bonding  $e_g$  complex), one of the main findings of Ref. 19, is clearly observed in our QSGW result. Another important feature in DMFT spectra is the ‘kink’ at around  $-0.2$  eV which compares well with the angle-resolved photoemission spectroscopy (ARPES) [23]. Noticeably, QSGW somehow captures such a feature: Compared to GGA, the reduced  $e_g$  bandwidth around the Fermi level results in the flattening of the band. In particular, the flat band along X- $\Gamma$  at around  $-0.6$  eV (see Fig. 2) is a shade of the ‘kink’ in DMFT and ARPES. Specifically, we note that the DMFT QP dispersion with  $\text{Im}\Sigma = 0^+$  goes to  $-0.6$  eV at the  $\Gamma$  point which is in good agreement with our QSGW dispersion. Mainly designed to construct the optimized QP picture, QSGW does not properly include the low energy magnetic fluctuation whereas the charge fluctuation is taken into account within RPA [24]. Therefore, by incorporating such an effect in the self-energy, we expect further flattening of the band and the kink-like structure, being more similar with ARPES and DMFT.

Importantly, our QSGW calculation of cubic LNO yields the well-converged PM solution. While LDA/GGA calculations ( $U=0$ ) predict the PM ground state for the bulk LNO, they significantly underestimate the correlation effects. On the other hand, the LDA/GGA+ $U$  calculation gives a magnetically ordered ground state which is in sharp contrast to the experiment. It demonstrates a clear limitation of the Hartree-Fock type of approach like LDA/GGA+ $U$  in the description of correlated PM phase. In this regard, QSGW has a definitely better aspect. Within the current implementation of QSGW, however, it is difficult to say that the PM phase is more stable energetically than the ferro (or anti-ferro) by com-

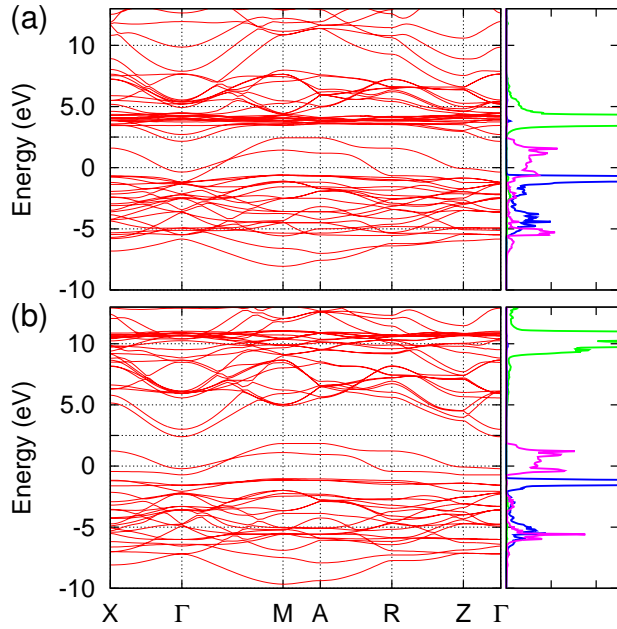


FIG. 3: The calculated band dispersion of LNO/LAO by (a) GGA and (b) QSGW. The Fermi level is set to be 0. The PDOS is also presented in the right panel in which the blue, magenta, and green lines refer to the Ni- $t_{2g}$ , Ni- $e_g$ , and La-4 $f$  states, respectively. The MT radii for Ni and La are the same with those in Fig. 1.

paring their total energies. We observed that a small difference in the computational settings can change the results regarding magnetic stability. It is basically a numerical instability and can be remedied in principle by improving our implementation [25]. At the same time, we presume that this instability is also related to the intrinsic magnetic instability of the system.

### B. Electronic structure of $(\text{LaNiO}_3)_1/(\text{LaAlO}_3)_1$

One of the most interesting issues in the LNO/LAO superlattice may be the Fermi surface topology. According to the DMFT calculation by Hansmann *et al.* [1], the inclusion of  $U$  causes the Fermi surface of LNO/LAO to be cuprate-like and only the  $d_{x^2-y^2}$  band is available around the Fermi energy. However, another DMFT calculation [2] arrived at a different conclusion. Based on the  $d$ - $p$  model which contains the oxygen bands explicitly in the DMFT procedure, Han *et al.* obtained a different spectra; *i.e.*, two  $e_g$  bands across the Fermi level and the central Fermi surface pocket is present even in the large  $U$  region. Since similarity or dissimilarity with the cuprate band structure was key to predicting possible high-temperature superconductivity in this superlattice, the correct description of electronic structures is of critical importance. The different conclusions by two DMFT calculations therefore require further examination. Also,

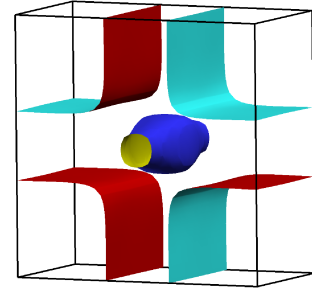


FIG. 4: The Fermi surface of LNO/LAO superlattice calculated by QSGW, which corresponds to the band dispersion of Fig. 2(b). The size of central pocket is slightly increased from the GGA result being consistent with Ref. [2].

the situation demonstrates the inherent ambiguity in the current DFT (density functional theory) +DMFT formalism; *e.g.*, the issues of double-counting, downfolding/projection, and the determination of  $U$  and  $J$ .

The QSGW method can be a good complementary choice as the fully charge self-consistent method with no adjustable parameter. The calculated band dispersion and the projected density of states (PDOS) are presented in Fig. 3. The GGA band in Fig. 3(a) compares well with the previous LDA or GGA calculations [8]. In the QSGW result presented in Fig. 3(b), two Ni- $e_g$  bands around the Fermi energy are reduced in their widths and separated from the Ni- $t_{2g}$  complex as observed in the bulk LNO (Fig. 1(b)). The bandwidth reduction is about 1.3 eV. In QSGW, the top of the Ni- $e_g$  bands are clearly lower than the bottom of the upper bands with a free electron-like feature around the  $\Gamma$  point. The La-4 $f$  level is pushed above from 4 to 10.5 eV as also noted in Fig. 1, and the core level bands are pushed down by  $\sim 3$  eV (not shown). The mass enhancement in the superlattice is comparable to that in LNO: The calculated effective electron and hole mass by QSGW are  $\sim 40$  and  $30$  % larger than the GGA values, respectively (see Table I).

Most importantly, the QSGW Fermi surface has the same topology as in GGA (see Fig. 4). The central Fermi surface still exists and the topology does not support the one-band physics of cuprates. The size of this central pocket is slightly increased from the GGA result, which is also observed in the DMFT calculation in Ref. [2]. This result is therefore consistent with the DMFT result of Ref. 2 rather than Ref. 1. Without any adjustable parameter or the ambiguity related to down-folding or double-counting, our QSGW results provide important new information for understanding the electronic structure and possible high-temperature superconductivity especially in the context of two previous DMFT studies yielding different conclusions.

Another interesting aspect of the nickelate superlattice is the MIT accompanied by the magnetic transition as observed by Boris *et al.* [3]. It is reported that



LNO/LAO becomes insulating and magnetic in the thin LNO limit. Since the LDA+ $U$  type of method predicts a magnetic solution even for the bulk LNO, its predictive power is questionable in the thin LNO superlattice although it actually gives the ferromagnetic ground state [9, 26]. On the other hand, LDA or GGA predicts the PM phase [8, 9] while DMFT calculations are mainly concerned with the PM region at high temperature [1, 2]. In this situation QSGW can also provide useful information. We found that the PM metallic phase is well stabilized in the QSGW calculation while the stability of the magnetic solution is questionable as in the case of bulk LNO (see Sec. III. A). The system is likely located in the vicinity of the magnetic instability. The calculated number of  $Ni_{e_g}$  electrons ( $N_{e_g}$ ), which can be an important indication for understanding MIT [27], is just slightly reduced by QSGW, as summarized in Table I.

#### IV. DISCUSSION

Since the important missing part in the QSGW QPs is mainly the magnetic fluctuation and its effects are largely for the near-Fermi energy, the overall band structure determined by QSGW should be acceptable. At the same time, however, the following points can be considered regarding the limitation of our calculations. First, structural distortions (such as  $GdFeO_3$ -type cage rotations and Jahn-Teller type), which were not taken into account in our calculation to reduce the computation cost, may be critically important. By reducing hopping, structural distortion can significantly enhance the electronic correlation. It is also noted that those distortions are actually found in the rare-earth nickelates, thin films and heterostructures [26, 28–30]. Second, although we failed to obtain a well-stabilized spin-polarized solution, it does not necessarily mean that the magnetic solution does not exist. Presumably the PM solution of QSGW is quite close to the magnetic phase boundary as discussed

above. Our guess is that the numerical instability found in our spin-polarized calculation is likely related to the intrinsic magnetic instability. Finally, the intrinsic limitation of QSGW itself is also noted. While the charge fluctuation is taken into account at the RPA level, the energy dependence of the self-energy is neglected during the self-consistency cycle. Therefore, further improvement to describe the correlation can be achieved, for example, in combination with DMFT [31].

#### V. SUMMARY

QSGW calculations have been performed to understand the electronic structure of LNO and the LNO/LAO superlattice. Without any *ad hoc* parameter or the ambiguity related to the double-counting and downfolding issue, the effects of correlation are well described in terms of the reduced bandwidth and the enhanced electron mass. Importantly, the Fermi surface topology does not become cuprate-like and one band physics is not achieved. This conclusion is consistent with a recent DMFT calculation based on the  $d$ - $p$  model and in a sharp contrast to the result from the  $d$ -band only model. The PM solution especially for the superlattice is presumably located in the vicinity of the magnetic instability, which possibly indicates the critical role of structural distortions in the local moment formation in this system.

#### VI. ACKNOWLEDGMENTS

We thank Prof. Hiroshi Katayama-Yoshida group at Osaka University for hosting the helpful discussion and allowing to use the cluster computers. This work was supported by ‘Core-to-Core Program on Computational Materials Design on Green Energy’.

- 
- [1] P. Hansmann, X. Yang, A. Toschi, G. Khaliullin, O. K. Andersen, and K. Held, *Phys. Rev. Lett.* **103**, 016401 (2009).
  - [2] M. J. Han, X. Wang, C. A. Marianetti, and A. J. Millis, *Phys. Rev. Lett.* **107** 206804, (2011).
  - [3] A. V. Boris, Y. Matiks, E. Benckiser, A. Frano, P. Popovich, V. Hinkov, P. Wochner, M. Castro-Colin, E. Detemple, V. K. Malik, C. Bernhard, T. Prokscha, A. Suter, Z. Salman, E. Morenzoni, G. Cristiani, H.-U. Habermeier, and B. Keimer, *Science* **332**, 937 (2011).
  - [4] N. Hamada, *J. Phys. Solids* **54** 1157 (1993).
  - [5] M. K. Stewart, J. Liu, M. Kareev, J. Chakhalian, and D. N. Basov, *Phys. Rev. Lett.* **107** 176401, (2011).
  - [6] J. Liu, S. Okamoto, M. van Veenendaal, M. Kareev, B. Gray, P. Ryan, J. W. Freeland, and J. Chakhalian, *Phys. Rev. B* **83** 161102, (2011).
  - [7] J. W. Freeland, J. Liu, M. Kareev, B. Gray, J.W. Kim, P. Ryan, R. Pentcheva, and J. Chakhalian, *EPL* **96** 57004, (2011).
  - [8] M. J. Han, C. A. Marianetti, and A. J. Millis, *Phys. Rev. B* **82** 134408 (2010).
  - [9] M. J. Han and M. van Veenendaal, *Phys. Rev. B* **85**, 195102 (2012).
  - [10] S. V. Faleev, M. van Schilfgaarde, and T. Kotani, *Phys. Rev. Lett.* **93**, 126406 (2004).
  - [11] M. van Schilfgaarde, T. Kotani, and S. Faleev, *Phys. Rev. Lett.* **96**, 226402 (2006).
  - [12] T. Kotani, M. van Schilfgaarde, and S. V. Faleev, *Phys. Rev. B* **76**, 165106 (2007).
  - [13] T. Kotani and M. van Schilfgaarde, *J. Phys.: Condens. Matter* **20**, 295214 (2008).
  - [14] A. N. Chantis, M. van Schilfgaarde, and T. Kotani, *Phys. Rev. B* **76**, 165126 (2007).
  - [15] T. Kotani and H. Kino, (unpublished).

- [16] T. Kotani and Mark van Schilfgaarde, Phys. Rev. B. **81**, 125117(2010)
- [17] T. Kotani and H. Kino, J. Phys. Soc. Jpn. **82**, 124714(2013)
- [18] D. R. Hamann, and D. Vanderbilt, Phys. Rev B **79**, 045109(2009)
- [19] X. Deng, M. Ferrero, J. Mravlje, M. Aichhorn, and A. Georges, Phys. Rev. B **85**, 125137 (2012).
- [20] G. Gou, I. Grinberg, A. M. Rappe, and J. M. Rondinelli, Phys. Rev. B **84**, 144101 (2011).
- [21] QSGW has a tendency to push down the localized bands relative to extended bands (see Ref. 12).
- [22] T. Kotani and H. Kino, J. Phys.: Condens. Matter **21**, 266002 (2009).
- [23] R. Eguchi, A. Chainani, M. Taguchi, M. Matsunami, Y. Ishida, K. Horiba, Y. Senba, H. Ohashi, and S. Shin, Phys. Rev. B **79**, 115122 (2009).
- [24] As in the case of phonon, the low magnetic fluctuation essentially affects the dispersion just near the Fermi energy. See, for example, C. Kirkegaard, T. K. Kim, and Ph. Hofmann, New J. Phys. **7**, 99 (2005).
- [25] For example, we expect that the inclusion of magnetic fluctuations on top of the paramagnetic solution of QSGW can give a reasonable description.
- [26] A. Blanca-Romero and R. Pentcheva, Phys. Rev. B **84**, 195450 (2011).
- [27] X. Wang, M. J. Han, L. de Medici, H. Park, C. A. Marianetti, and A. J. Millis, Phys. Rev. B **86**, 195136 (2012).
- [28] M. Imada, A. Fujimori, and Y. Tokura, Rev. Mod. Phys. **70**, 1039 (1998).
- [29] J. Chakhalian, J. M. Rondinelli, J. Liu, B. A. Gray, M. Kareev, E. J. Moon, N. Prasai, J. L. Cohn, M. Varela, I. C. Tung, M. J. Bedzyk, S. G. Altendorf, F. Strigari, B. Dabrowski, L. H. Tjeng, P. J. Ryan, and J. W. Freeland Phys. Rev. Lett. **107**, 116805 (2011).
- [30] H. -S. Kim and M. J. Han, arXiv:1306.0713 (2013).
- [31] J. M. Tomczak, M. van Schilfgaarde, and G. Kotliar, Phys. Rev. Lett. **109**, 237010 (2012)